PNAS RESEARCH ARTICLE | CHEMISTRY

Low-temperature gas-phase formation of cyclopentadiene and its role in the formation of aromatics in the interstellar medium

Zhenghai Yang[a], Iakov A. Medvedkov[a], Shane J. Goettl[a], Anatoliy A. Nikolayev[b], Alexander M. Mebel[c], Xiaohu Li[d,e,f,1], and Ralf I. Kaiser[a,1]

Affiliations are included on p. 9.

Edited by F. Fleming Crim, University of Wisconsin–Madison, Madison, WI; received May 17, 2024; accepted November 2, 2024

The cyclopentadiene (C_5H_6) molecule has emerged as a molecular building block of nonplanar polycyclic aromatic hydrocarbons (PAHs) and carbonaceous nanostructures such as corannulene ($C_{20}H_{10}$), nanobowls ($C_{40}H_{10}$), and fullerenes (C_{60}) in deep space. However, the underlying elementary gas-phase processes synthesizing cyclopentadiene from acyclic hydrocarbon precursors have remained elusive. Here, by merging crossed molecular beam experiments with rate coefficient calculations and comprehensive astrochemical modeling, we afford persuasive testimony on an unconventional low-temperature cyclization pathway to cyclopentadiene from acyclic precursors through the reaction of the simplest diatomic organic radical—methylidyne (CH)—with 1,3-butadiene (C_4H_6) representing main route to cyclopentadiene observed in TaurusMolecular Cloud. This facile route provides potential solution for the incorporation of the cyclopentadiene moiety in complex aromatic systems via bottom–up molecular mass growth processes and offers an entry point to the low-temperature chemistry in deep space leading eventually to nonplanar PAHs in our carbonaceous Universe.

reaction dynamics | five-membered ring | polycyclic aromatic hydrocarbon | interstellar medium | aromaticity

Significance

Since the detection of benzonitrile (C_6H_5CN) and cyanonaphthalene ($C_{10}H_7CN$) in Taurus Molecular Cloud (TMC-1), mankind has witnessed a rapid expansion of the chemistry of aromatics in cold molecular clouds. Despite the acceptance of aromatics being widespread in the interstellar medium, little is known on their fundamental formation mechanisms. Exploiting cyclopentadiene (C_5H_6) as a benchmark, we demonstrate that aromatics identified in TMC-1 can be efficiently formed in a bottom–up synthesis from acyclic precursors via bimolecular reactions commencing with methylidyne (CH) and 1,3-butadiene (C_4H_6) readily available in TMC-1. These findings open up a versatile concept to efficiently connect five-membered ring and aromatic chemistries in deep space, thus expanding our fundamental knowledge on the chemical evolution of the interstellar medium.

For several decades, cold molecular clouds such as the Taurus Molecular Cloud (TMC-1) have been recognized as natural laboratories and molecular factories on the macroscopic scale for fostering our fundamental understanding of molecular mass growth processes through astronomical observations merged with astrochemical modeling capitalizing on complex gas-phase reaction networks of ion–molecule and neutral–neutral reactions (1–7). Triggered by the identification of cyclopropenylidene (C_3H_2) (8–10), the first observed interstellar hydrocarbon ring, and a series of nonaromatic and aromatic hydrocarbon cycles including cyclopentadiene (C_5H_6) (9, 10), benzene (C_6H_6) (11), indene (C_9H_8) (12, 13), naphthalene ($C_{10}H_8$) (14), and their cyano (CN) or ethynyl (CCH) substituted species (13, 15, 16) with significant fractional abundances up to 10^{-8} relative to molecular hydrogen, particular attention has been devoted to the underlying elementary processes transforming acyclic hydrocarbons to hydrocarbon rings and to polycyclic aromatic hydrocarbons (PAHs) (11, 17). Among these hydrocarbons, the cyclopentadiene molecule (C_5H_6) has emerged as a critical precursor to aromatic molecules carrying five-membered rings such as indene (C_9H_8) and 1-indenyl ($C_9H_7^{\bullet}$) radical representing molecular building blocks to rationalize the formation of nonplanar, bowl-shaped aromatic hydrocarbons such as corannulene ($C_{20}H_{10}$) and nanobowls ($C_{40}H_{10}$) (Fig. 1) (18–20). However, a detailed understanding of the molecular mass growth processes to nonplanar, aromatic hydrocarbons has to commence with the elucidation of the key route to the very basic building block - cyclopentadiene (C_5H_6) - from acyclic precursors. The lack of documented gas-phase formation routes to cyclopentadiene (C_5H_6) resulted in contemporary astrochemical models unable to account for the occurrence of ubiquitous cyclopentadiene (C_5H_6) in TMC-1 with astrochemical models predicting fractional abundances up to three orders of magnitude below astronomical observations (6). Therefore, key synthetic routes to cyclopentadiene (C_5H_6) under the low-temperature conditions of TMC-1 of 10 K are clearly lacking, but fundamental to the astrochemistry communities to ultimately untangle prevailing molecular mass growth processes driving the formation of complex PAHs and eventually fullerenes (C_{60} and C_{70}) and carbonaceous grains (21).

Combining molecular beams experiments with theoretical kinetics calculations and astrochemical modeling, we reveal here the previously elusive gas-phase formation routes to cyclopentadiene (C_5H_6) in TMC-1 via the reaction of the simplest diatomic organic radical—methylidyne (CH)—with 1,3-butadiene (C_4H_6). The bimolecular, barrierless

The authors declare no competing interest.

This article is a PNAS Direct Submission.

[1]To whom correspondence may be addressed. Email: xiaohu.li@xao.ac.cn or ralfk@hawaii.edu.

This article contains supporting information online at https://www.pnas.org/lookup/suppl/doi:10.1073/pnas.2409933121/-/DCSupplemental.

Published December 11, 2024.

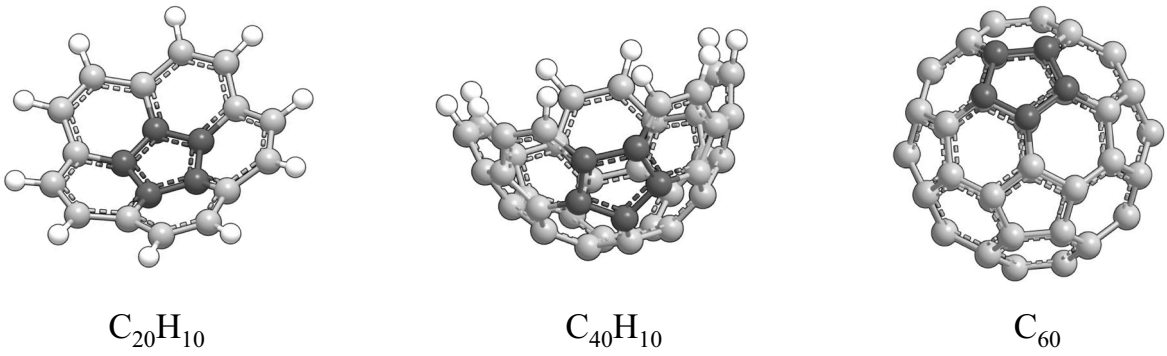

Fig. 1. Molecular structures of 3-dimensional carbonaceous nanostructures. Molecular structures of corannulene ($C_{20}H_{10}$), C40-nanobowl ($C_{40}H_{10}$), and buckminsterfullerene (C_{60}). The carbon atoms of the cyclopentadiene moiety are highlighted in black; the remaining carbon and hydrogen atoms are color coded in gray and white, respectively.

reaction is rapid at low temperatures prevailing in molecular clouds such as TMC-1 and can deliver the cyclic cyclopentadiene (C_5H_6) molecule from acyclic precursors under single collision conditions in the gas phase. Astrochemical models reveal the key role of cyclopentadiene (C_5H_6) in the synthesis of aromatics and their substituted counterparts such cyano- and ethynyl- derivatives by simultaneously predicting and replicating astronomically observed hydrocarbons and their nitriles in TMC-1. These findings offer a unique entry point of cyclopentadiene to the low-temperature chemistry in deep space leading eventually to nonplanar PAHs, thus providing a comprehensive understanding of the chemical evolution of carbonaceous Universe we live in.

Results

Laboratory Frame. The reactive scattering experiments of the CH ($X^2\Pi$) and d1-methylidyne (CD, $X^2\Pi$) radicals with C_4H_6 (X^1A_g) were studied in the gas phase under single collision conditions (*SI Appendix*, Table S1). In the CH (13 amu)—$CH_2CHCHCH_2$ (54 amu) system, reactive scattering signal was detected at mass-to-charge (*m/z*) ratios of 67 ($C_5H_7^+/^{13}CC_4H_6^+$), 66 ($C_5H_6^+/^{13}CC_4H_5^+$), and 65 ($C_5H_5^+/^{13}CC_4H_4^+$). Weak signal at m/z = 67 was integrated to be only 7 ± 2% compared to ion counts at *m/z* = 66. After scaling, the time-of-flight (TOF) spectra of all mass-to-charge ratios (67, 66, 65) overlap. These findings indicate a single reaction channel via atomic hydrogen loss (*m/z* = 66) with signal at *m/z* = 67 originating from natural isotope abundance of carbon (^{12}C 98.9%, ^{13}C 1.1%) [reaction (1)]; ion counts at *m/z* = 65 arise from dissociative electron impact ionization of the neutral C_5H_6 parent in the electron impact ionizer. Since ion counts at *m/z* = 66 are collected at a level of only 45 ± 4% compared to its fragment at *m/z* = 65, TOFs were recorded at *m/z* = 65 in 2.5° intervals from 15° to 66°. The TOFs were then integrated and normalized with respect to the signal at the center-of-mass angle, thus yielding the laboratory angular distribution (LAD); the latter features a broad distribution exceeding 50° and a forward-backward symmetry around the CM angle. These findings propose indirect reaction dynamics through the involvement of C_5H_7 intermediate(s) prior to dissociating to C_5H_6 isomer(s) plus atomic hydrogen.

The CD—C_4H_6 reaction was conducted to evaluate the effect of the deuterated CH reactant on the reaction dynamics. Reactive scattering signal was detected at *m/z* = 68 ($C_5H_6D^+/^{13}CC_4H_5D^+$), 67 ($C_5H_5D^+/^{13}CC_4H_4D^+/^{13}CC_4H_6^+$), 66 ($C_5H_4D^+/C_5H_6^+/^{13}CC_4H_3D^+/^{13}CC_4H_5^+$), and 65 ($C_5H_3D^+/C_5H_5^+/^{13}CC_4H_2D^+/^{13}CC_4H_4^+$). A close look at these spectra suggests the best signal-to-noise ratio at *m/z* = 66 with ion counts at *m/z* = 67 and 65 collected at a level of 51 ± 4% and 17 ± 3%, respectively, compared to *m/z* = 66. Indistinguishable patterns of these TOFs are exhibited after scaling; similar ratios of the ion count at *m/z* = 66 versus *m/z* = 65 (CH—C_4H_6) of 0.45 ± 0.04: 1 and *m/z* = 67 versus *m/z* = 66 (CD—C_4H_6) of 0.51 ± 0.04: 1 suggest the prevalence of the CD versus atomic hydrogen exchange pathway accompanied by the gas-phase preparation of molecule(s) with the formula C_5H_5D (67 amu) with the atomic hydrogen atom loss originating from the C_4H_6 reactant. The atomic deuterium loss channel is—if at all—only of minor importance. Further, ion counts at m/z = 68, 66, and 65 can be accounted through the natural abundance of ^{13}C ($^{13}CC_4H_5D^+$; *m/z* = 68) and dissociative electron impact ionization of the neutral C_5H_5D in the electron impact ionizer (m/z = 66, 65). Subsequently, TOF spectra are collected at *m/z* = 66 and scaled to extract the LAD (Fig. 2). Similar to the CH—C_4H_6 system, this distribution is forward-backward symmetric inferring indirect reaction dynamics through the formation of chemically activated intermediates (C_5H_6D) (22–24).

Center-of-Mass Frame. With the identification of the atomic hydrogen loss channel in both the CH—C_4H_6 and CD—C_4H_6 systems along with the gas-phase preparation of C_5H_6 and C_5H_5D isomer(s), respectively, we are elucidating the nature of the C_5H_6/C_5H_5D isomer(s) together with the underlying mechanisms of their formation (25). This is accomplished by converting the laboratory data (TOFs, LAD) into the CM reference frame. First, for the CH—C_4H_6 system, best fits of the laboratory data are achieved with a single reaction channel [reaction (1)]. All attempts to reproduce the experimental data with a molecular hydrogen loss channel failed, confirming the existence of only H loss channel leading to the product isomer(s) with the formula of C_5H_6. Second, for the CD—C_4H_6 reaction, considering that atomic H/D might emit from C_4H_6/CD reactants under experimental conditions, both atomic H and D loss channels need to be examined. As depicted in Fig. 3, the laboratory data could also be replicated through a single atomic hydrogen loss [reaction (2a)]. Note that in order to investigate the contribution of atomic D loss channel to the collected signal, we also attempted to fit the laboratory data at *m/z* = 66 with two channels: an atomic hydrogen loss channel [reaction (2a)] and an atomic deuterium loss channel (D) [reaction (2b)]. However, only contributions of up to 7% from the atomic deuterium channel can be accounted for. Consequently, the best-fit CM functions, $P(E_T)$ and $T(\theta)$, for both systems are attained via single atomic hydrogen loss channel (Fig. 3). The $P(E_T)$ prolongs to maximum (E_{max}) kinetic energy releases of 352 ± 22 and 357 ± 23 kJmol^{-1}, respectively, for the formation C_5H_6 [reaction (1)] and C_5H_5D [reaction (2a)]. These energies can be utilized to recover the reaction energies via the relationship of $E_{max} = E_C - \Delta_r G$ for product(s) born without internal excitation

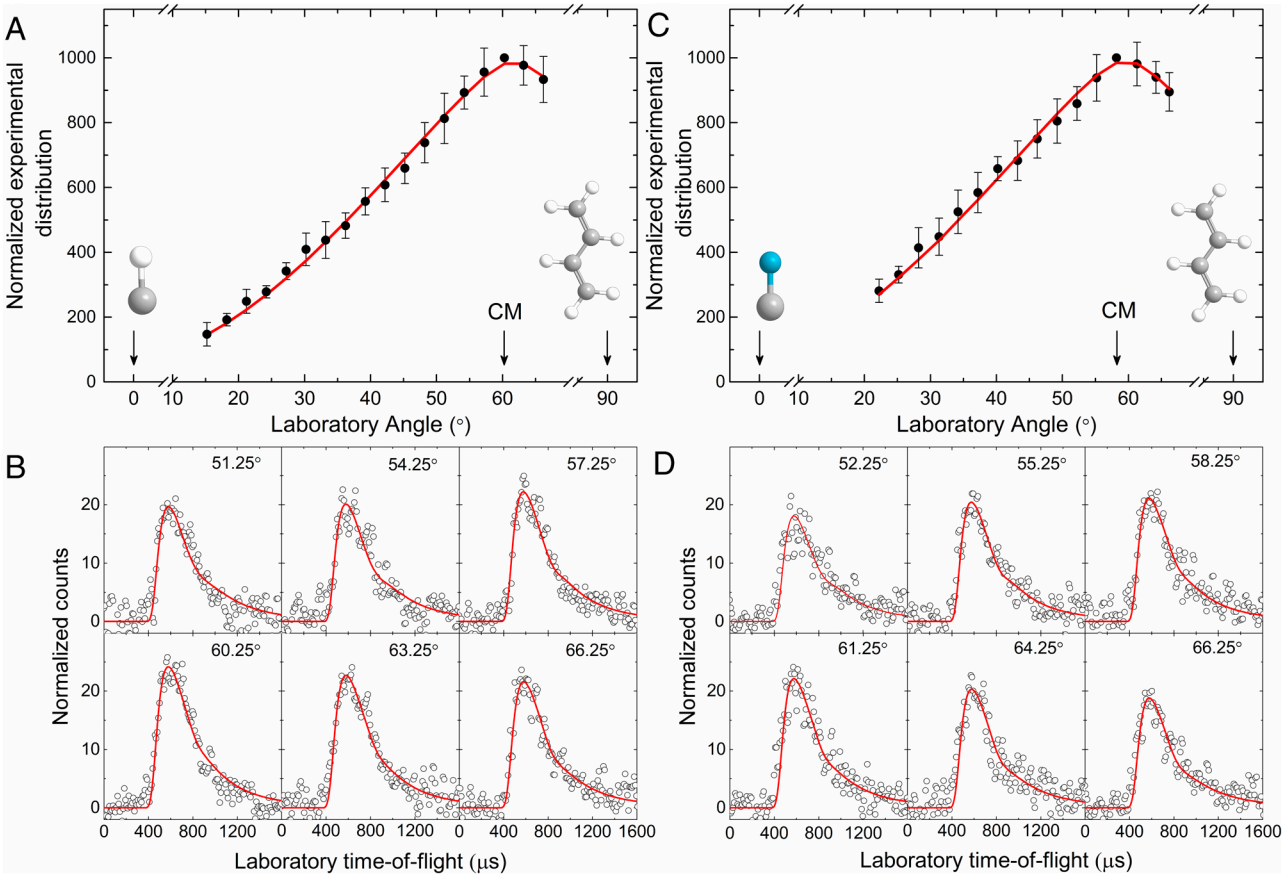

Fig. 2. Laboratory data for the CH—C_4H_6 and CD—C_4H_6 systems. LAD and TOFs for the reactions of CH and CD radicals with C_4H_6. Data are collected at m/z = 65 (*A* and *B*) and 66 (*C* and *D*) for the CH—C_4H_6 and CD—C_4H_6 system, respectively. The solid and open circles define the experimental data, and the red line represents the best fits. Colors of the atoms: carbon, gray, hydrogen, white, deuterium, light blue.

with the collision energy E_C. Consequently, experimental reaction exoergicities of 346 ± 22 kJmol^{-1} (CH—C_4H_6) and 350 ± 23 kJmol^{-1} (CD—C_4H_6) are obtained considering the corresponding collision energy E_C of 6.2 ± 0.3 and 6.5 ± 0.3 kJmol^{-1}, respectively. These values agree nicely with The Active Thermochemical Tables from Argonne in Chicago reaction energy of 355 ± 2 kJ mol^{-1} to form the cyclopentadiene isomer along with atomic hydrogen (26, 27). Both distributions peak well away from zero translational energy (85 ± 5 kJ mol^{-1}) signifying that C_5H_7 and C_5H_6D reaction intermediates decompose via tight exit transition states, i.e., a process connected with an extensive rearrangement of the electron density from the reaction intermediate to the final products. Additionally, the average translational energies of the products are calculated to be 131 ± 8 kJ mol^{-1} for both systems suggesting that 37 ± 5% of the available energy is released into the translational degrees of freedom of the products. Let us now inspect the center-of-mass angular distributions. Both $T(\theta)$s are forward-backward symmetric with pronounced maxima at 90° indicating that the reactions proceed through indirect scattering dynamics via the involvement of C_5H_7 and C_5H_6D complex(es) possessing lifetime(s) longer than the corresponding rotational period (22); the CM angular distributions peaks at 90° is also indicative of geometrical constraints upon decomposition of the C_5H_7 and C_5H_6D intermediates with an emission of the atomic hydrogen nearly perpendicularly to the rotation plane of the decomposing complex (28). These findings are also reflected in the flux contour maps, which reveals overall images of scattering processes.

$$\mathrm{CH\,(13\,amu) + C_4H_6\,(54\,amu) \rightarrow C_5H_6\,(66\,amu) + H\,(1\,amu),} \quad [1]$$

$$\mathrm{CD\,(14\,amu) + C_4H_6\,(54\,amu) \rightarrow C_5H_5D\,(67\,amu) + H\,(1\,amu),} \quad [2]$$

$$\mathrm{CD\,(14\,amu) + C_4H_6\,(54\,amu) \rightarrow C_5H_6\,(66\,amu) + D\,(2\,amu).} \quad [3]$$

Discussion

Reaction Mechanism. With the detection of C_5H_6 and C_5H_5D isomers along with compelling evidence of the atomic hydrogen elimination from the C_4H_6 reactant, we are now combining these results with electronic structure calculations to extract the nature of the isomers formed and to address the underlying reaction mechanisms (Fig. 4 and *SI Appendix*, Figs. S1 and S2) (29); statistical calculations exploiting Rice–Ramsperger–Kassel–Marcus (RRKM) theory to predict the branching ratios computationally were also conducted for 10 K (*SI Appendix*, Tables S2–S4). First, C_4H_6 can exist in its *s-trans* and *s-cis*/*gauche* forms and *s-trans*-C_4H_6 is more stable by about 12 kJ mol^{-1} as compared to the *s-cis*/*gauche* conformers. Both isomers can be interconverted but a high barrier of around 23.5 kJ mol^{-1} is involved. Under our experimental conditions, 99.6% of the C_4H_6 reactant exists in the energetically more stable *s-trans* form (30–32). Importantly, the experimentally derived reaction energy

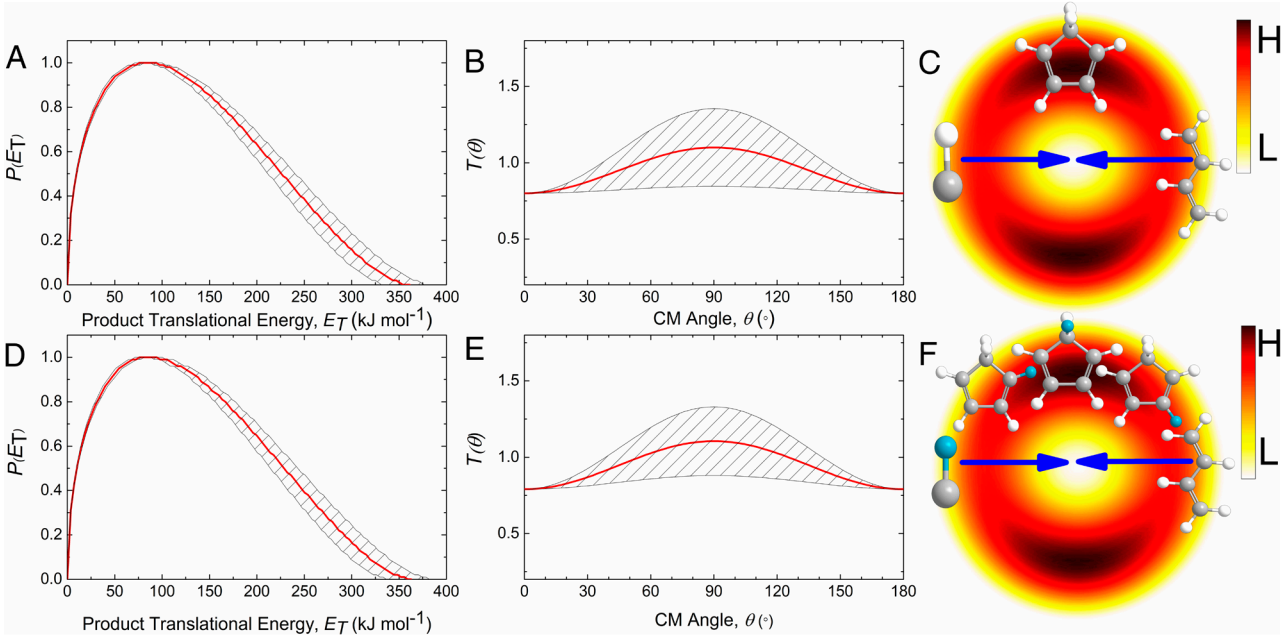

Fig. 3. CM functions for the CH—C_4H_6 and CD—C_4H_6 systems. CM translational energy, angular flux distribution, and the corresponding flux contour map for the reaction of C_4H_6 with CH (*A*–*C*) and CD (*D*–*F*). The red lines represent the best fit, and the shaded area depicts the error limits of the best fits.

of 346 ± 22 kJ mol^{-1} correlates nicely with the computationally predicted reaction energy of 349 ± 8 kJ mol^{-1} for forming the thermodynamically most stable cyclopentadiene isomer (**p1**). The accuracy of theoretical calculations is taken from the assessment in the literature where the theoretical methods used here were tested in terms of comparison with experimental data including relative energies of different isomers, reaction energies, and barrier heights (33). However, higher energy isomers **p2** and **p3** cannot be excluded at this stage since their contributions might be masked in the low energy section of the $P(E_T)$. Key reaction pathways leading to **p1** (cyclopentadiene, $^1A_1$, C_{2v}), **p2** (trans-3-vinyl-cyclopropene, $^1A'$, C_s, −135 kJ mol^{-1}), and **p3** (cis-3-vinyl-cyclopropene, $^1A'$, C_s, −130 kJ mol^{-1}) isomers are compiled in Fig. 4. The CH–C_4H_6 reaction can be initiated via five barrierless entrance channels: addition of CH radical to the terminal carbon atom (I) or to the carbon–carbon double bond (II) insertion into the terminal C—H bond (III) or the carbon–carbon single bond (IV). These pathways access five initial intermediates: **i1** (I, −130 kJ mol^{-1}),

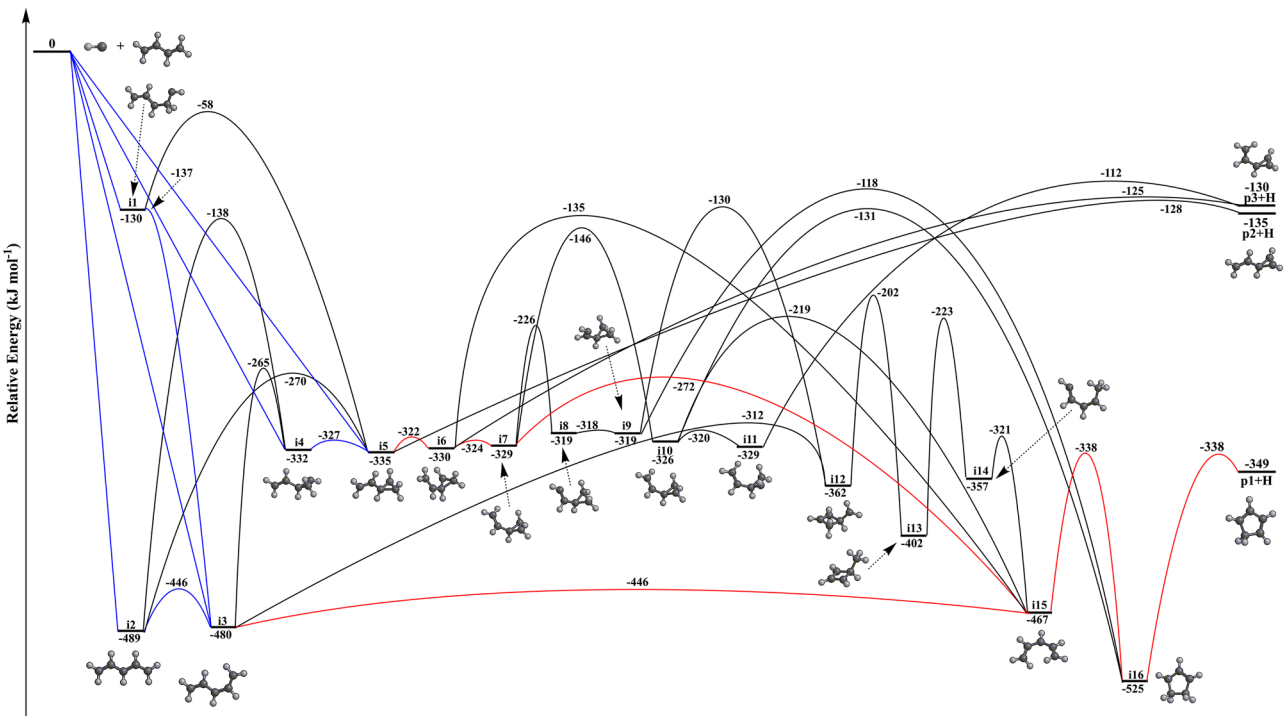

Fig. 4. Potential energy surface (PES) for the CH—C_4H_6 reaction. Selected pathways from the PES (ref. 29) include those leading to cyclopentadiene (p1), trans- (p2), and cis-3-vinyl-cyclopropene (p3). The blue lines represent the isomerization among the initial adducts of **i1**–**i5** and the red lines depict the most important pathways to p1.

i2 (III/IV, −489 kJ mol^{-1}), **i3** (III/IV, −480 kJ mol^{-1}), and **i4**/**i5** (II, −332/−335 kJ mol^{-1}). The adduct **i1** is metastable as the transition state for a [1,2]-H migration to **i3** found at the DFT level of geometry optimization falls 7 kJ mol^{-1} below **i1** at the higher level of theory (29). Alternatively, ring closure of **i1** to **i5** requires a barrier of 72 kJ mol^{-1} to be overcome. Ring closure in **i2** leads to **i4** or **i5**, which are connected via a low barrier of 5 kJ mol^{-1}. The collision complex **i2** can isomerize via a barrier of 43 kJ mol^{-1} to **i3**, which is connected to **i4** through a barrier of 215 kJ mol^{-1}. Considering these isomerization processes among the five initial adducts **i1**–**i5** (Fig. 4; blue pathways), the energetically preferred pathways may involve the formation of equilibrated mixtures of **i2**/**i3** and **i4**/**i5**. What is the fate of these intermediates? **i3** preferentially undergoes trans–cis isomerization to **i15** rather than ring-closure to **i12**. A subsequent cyclization to **i16** and hydrogen atom loss from the CH_2 moiety in **i16** provides **p1**. As for **i5**, the isomerization sequence to **i6** and **i7** involving rotations around single C—C bonds can proceed via low barriers of only 13 and 6 kJ mol^{-1}. Once formed, **i7** can further rearrange through ring-opening to the acyclic intermediate **i15**. Hence, overall two distinct routes connect **i3** and **i5** to **i15** and eventually **p1**. These are **i5** → **i6** → **i7** → **i15** → **i16** → **p1**+H and **i3** → **i15** → **i16** → **p1**+H (Fig. 4; red lines).

The results for the CD—C_4H_6 system provide additional constrains on the underlying reaction mechanism(s) (*SI Appendix*, Fig. S2). Here, the CD radical can be exploited to trace the deuterium versus hydrogen atoms in distinct reaction intermediates. Effectively, addition and/or insertion pathways of CD de facto incorporate the deuterium atom within a three-membered ring (**i4**/**i5**), terminal CD (**i1**) or CHD moieties (**i2**/**i3**), or the central CD group (**i2**/**i3**). The latter possibility can be realized only upon a CD insertion into the single C—C bond in C_4H_6 which is less likely than the insertion into a C—H bond. Successive isomerization eventually provides three distinct isotopomers of **i16**, which then undergo unimolecular decomposition via elimination of atomic hydrogen or deuterium to distinct isotopomers of **p1**. Note that atomic deuterium can only be eliminated from the CHD group in **i16**; atomic hydrogen can be eliminated from 11 positions in the CH_2 groups considering three different isotopomers of **i16**. Therefore, within statistical limits, only 8% of cyclopentadiene is expected to be formed via atomic deuterium loss, while 92% are accessed through the loss of atomic hydrogen. This is well supported through the laboratory data within the CD—C_4H_6 system revealing upper limits of the deuterium loss of only 7%. Recall that **p2**/**p3** can also be generated through H/D loss from the CH_2/CHD group of the three-membered rings of **i5**, **i6**, or **i11** with a statistical ratio of 1:5 for deuterium versus hydrogen, i.e., 17% of vinylcyclopropene are formed via atomic deuterium loss. As discussed above, this is not supported by our experimental findings.

Overall, our combined experimental and computational results certify the formation of cyclopentadiene (C_5H_6) and d1-cyclopentadiene (C_5H_5D) involving two pathways **i3** → **i15** → **i16** → **p1**+H and **i5** → **i6** → **i7** → **i15** → **i16** → **p1**+H; these findings are fully supported by statistical calculations carried out for five initial intermediates (**i1** – **i5**) within the premise of a complete energy randomization (*SI Appendix*, Table S2). At our collision energy of 6.2 kJ mol^{-1}, **p1** is the dominant product with the contribution of 75%; a reduction of the collision energy to 0 kJ mol^{-1} has only a marginal effect on the yield of **p1** (77%). These computations further reveal that starting from **i1** to **i3**, 98% of **p1** is

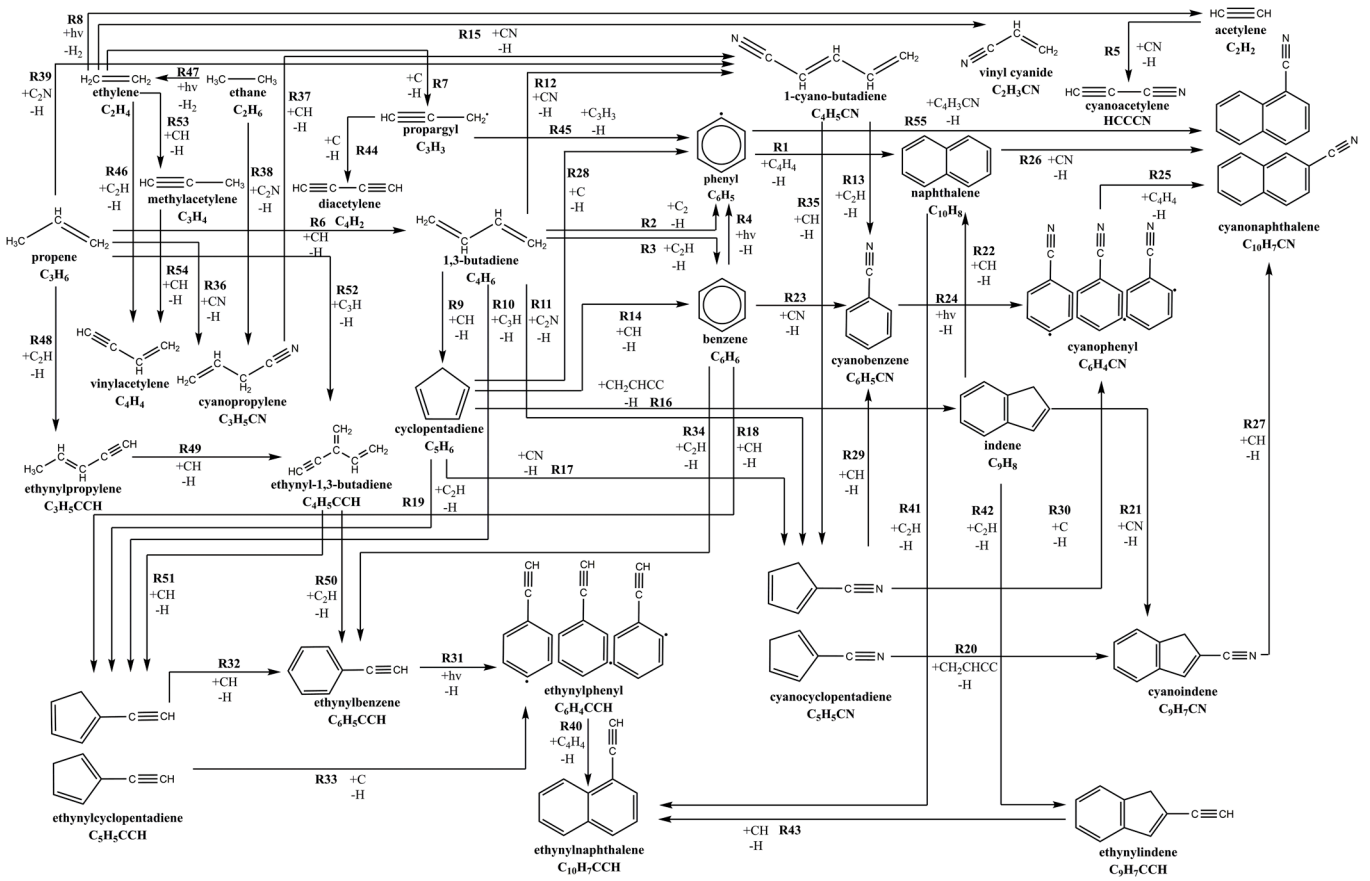

Fig. 5. Reaction network forming ring molecules in TMC-1. Compilation of key bimolecular reactions incorporated into the astrochemical modeling leading to cyclopentadiene (C_5H_6) and more complex ring molecules.

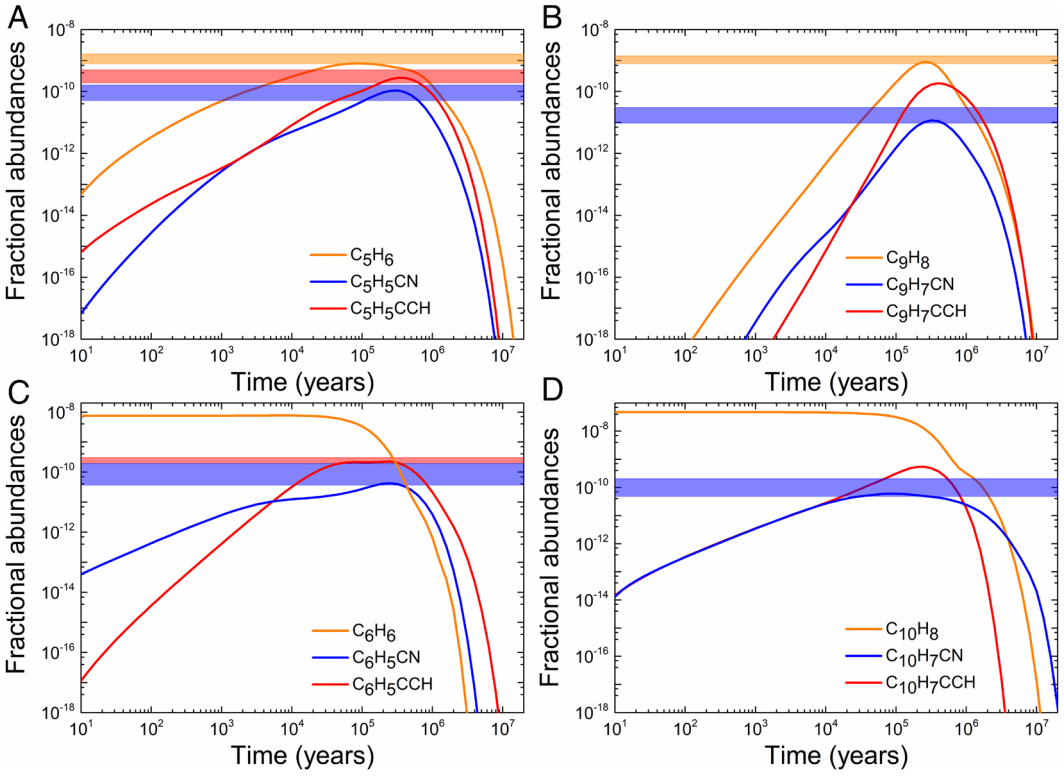

Fig. 6. Results of the astrochemical model for TMC-1. The fractional abundances of the unsubstituted prototype mono- and bicyclic molecules involving five- and six-membered rings of cyclopentadiene (C_5H_6, *A*), indene (C_9H_8, *B*), benzene (C_6H_6, *C*), and naphthalene ($C_{10}H_8$, *D*) are plotted as a function of time and color-coded in orange. The blue and red lines in each figure represent the corresponding CN and CCH substituted species. The astronomically observed fractional abundances along with the uncertainties are visualized by orange, red, and blue colored horizontal bars.

formed via the **i3** → **i15** → **i16** → **p1**+H pathway. Both experiments and computations support a dominant formation of cyclopentadiene via the exoergic and barrierless bimolecular reaction of CH radicals with C_4H_6 involving the key reaction sequence **i3** → **i15** → **i16** → **p1**+H through indirect scattering dynamics. The computationally predicted tight exit transition state is supported by our experimental findings, i.e., a center-of-mass angular distribution peaking away from zero translational energy. Further, the sideway scattering reflected in the center-of-mass angular distribution is also evident from the computed structure of the transition state associated with **i16**→**p1**+H (*SI Appendix*, Fig. S3), in which the hydrogen atom emitting nearly perpendicularly to the rotational plane of the decomposing complexes at 83°. Finally, we would like to stress that the experimental results (LAD, TOFs) and the derived CM functions of the CD—C_4H_6 reaction depict nearly the same pattern as for the CH—C_4H_6 system, which also verifies the dominant formation of d1-cyclopentadiene (C_5H_5D) with an atomic hydrogen loss from C_4H_6. It is important to note that the outcome of the reactions dramatically changes with the collision energy. At a collision energy of 20.8 kJ mol^{-1}, only **p2** and **p3** products were identified (29). The non-RRKM behavior at elevated collision energies can be rationalized by lifetime(s) of the reaction intermediates being too low to allow a complete energy randomization to occur. These findings suggest distinct, collision-energy-dependent chemical dynamics promoting ring-closure and efficient, barrierless formation of the five-membered ring molecule cyclopentadiene (C_5H_6) as the collision energy drops.

Astrochemical Modeling. Having provided a solid experimental proof on the gas-phase preparation of cyclopentadiene (C_5H_6) via the barrierless reaction of the CH with C_4H_6, we deliberate on the potential astrochemical implications. The computations have revealed explicitly that the CH—C_4H_6 reaction is exoergic and has no entrance barrier, and all barriers involved in the formation of cyclopentadiene (C_5H_6) are well below the energy of the separated reactants. These results represent crucial requirements for this reaction to be open in low-temperature conditions such as cold molecular clouds with temperature as low as 10 K. The fact that CH reacts with unsaturated and saturated hydrocarbons without a barrier and with high rate coefficients close to the gas-kinetic limit at extremely low temperatures is supported not only by our electronic structure calculations but also by previous experimental and theoretical studies (34–38). Exploiting astrochemical modeling, these studies are now expanded to simulate the "real" chemical complexity of cold molecular clouds by transferring these results from the laboratory to TMC-1. This is of central importance since despite their ubiquity in TMC-1, the low-temperature preparation and chemical evolution of cyclic hydrocarbons such as cyclopentadiene (C_5H_6) (9) and indene (C_9H_8) (13)—the simplest aromatic molecule carrying a cyclopentadiene moiety—remained poorly constrained. Both cyclopentadiene (C_5H_6) and indene (C_9H_8) are weakly polar with dipole moments of 0.42 D (39) and 0.50 D (40) and were detected in TMC-1 with rich fractional abundances of (8 to 16) × 10^{-10} and (8 to 14) × 10^{-10} relative to molecular hydrogen (10, 12, 15), thus representing the most abundant ring molecules in the gas phase in cold molecular clouds detected to date. However, the formation pathways to cyclic hydrocarbons such as cyclopentadiene are completely lacking. As the direct consequence of incomplete chemical networks of the contemporary astrochemical modeling, the fractional abundances of key aromatics identified recently in TMC-1 are significantly underestimated (6, 12) with 1- and 2-cyanonaphthalene ($C_{10}H_7CN$) underpredicted by more than three orders of magnitude due to the incomplete reaction network previously exploited (*SI Appendix*, Fig. S4) (6).

Under the low-density conditions (10^4 to 10^6 cm^{-3}), bimolecular reactions drive the chemistry; likewise, the low temperature

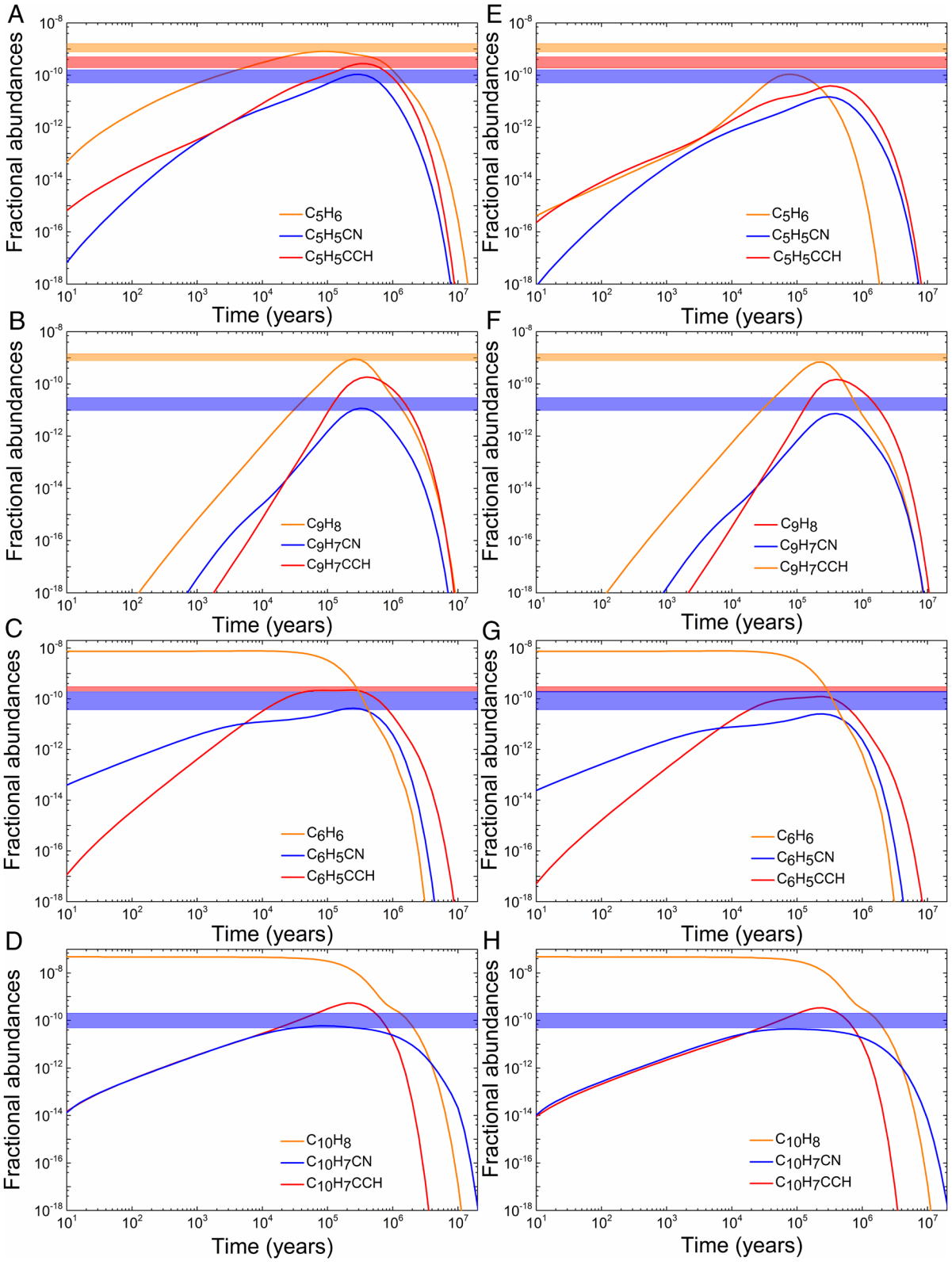

Fig. 7. Outcome of the modeling with the CH—C_4H_6 reaction (*A*–*D*) and the test modeling (*E*–*H*) which excluded the CH—C_4H_6 reaction are depicted.

of typically 10 K excludes bimolecular reactions with entrance barriers (35). To explore the overall efficiency of CH—C_4H_6 reaction in the formation of cyclopentadiene (C_5H_6) in the cold molecular clouds of TMC-1, a two-step single-point time-dependent astrochemical modeling was operated exploiting a revised UMIST (University of Manchester Institute of Science and Technology) Database (41). Physical parameters are based on refs. 19, 41, and 42: a temperature of 10 K, a cosmic ray ionization rate of 1.3×10^{-17} s^{-1}, a number density of molecular hydrogen of 10^4 cm^{-3}, and a visual extinction of 10 Mag. The chemical network was enhanced with rapid and barrierless reactions leading to the formation of cyclopentadiene (C_5H_6) (10, 16), benzene

(C_6H_6) (11), indene (C_9H_8) (12), naphthalene ($C_{10}H_8$) (14), and their cyano (CN) or ethynyl (CCH) substituted species identified recently (Fig. 5 and *SI Appendix*, Table S5) (10, 13, 16). The performance of this model are demonstrated by comparing the modeled fractional abundance with the astronomically observed values (*SI Appendix*).

Our modeling studies unravel captivating findings (Fig. 6). *First*, as depicted in Fig. 6 *A* and *B*, the predicted peak abundances of $(8.1 \pm 0.4) \times 10^{-10}$ at 8.0×10^4 y and $(9.0 \pm 0.4) \times 10^{-10}$ at 2.5×10^5 y for cyclopentadiene (C_5H_6) and indene (C_9H_8) agree well with the astronomically abundances of $(8 - 16) \times 10^{-10}$ (10, 16) and $(8 - 14) \times 10^{-10}$, respectively (12, 13). The central role of CH—C_4H_6 reaction in forming cyclopentadiene (C_5H_6) in TMC-1 is directly reflected by operating a model which excluded the title reaction. In this scenario, the peak fractional abundances of C_5H_6 decrease to only $(1.1 \pm 0.2) \times 10^{-10}$, indicating that cyclopentadiene is formed predominantly via the CH—C_4H_6 reaction (Fig. 7). These results support that the CH+C_4H_6 reaction is the important source of the observed cyclopentadiene in TMC-1, other reactions including C_2H+C_3H_6 might represent the minor source. The fractional abundances of cyano (CN) and ethynyl (CCH) substituted cyclopentadiene (C_5H_6) and indene (C_9H_8) including cyanocyclopentadiene (C_5H_5CN), ethynylcyclopentadiene (C_5H_5CCH), and cyanoindene (C_9H_7CN) are also well replicated (*SI Appendix*). *Second*, benzene (C_6H_6) and naphthalene ($C_{10}H_8$) are nonpolar and hence cannot be detected via radioastronomical techniques. Nevertheless, the detected rich abundances of their cyano (CN) and ethynyl (CCH) substituted proxies in TMC-1 indicate that benzene (C_6H_6) and naphthalene ($C_{10}H_8$) represent an "invisible" and critical reservoir (Fig. 6 *C* and *D*) (43, 44). Here, peak abundances of cyanobenzene (C_6H_5CN), ethynylbenzene (C_6H_5CCH), and cyanonaphthalene ($C_{10}H_7CN$) are predicted to be $(4.2 \pm 0.5) \times 10^{-11}$, $(2.2 \pm 0.3) \times 10^{-10}$, and $(6.0 \pm 0.5) \times 10^{-11}$, thus replicating the astronomical observations nicely [$(4 - 20) \times 10^{-11}$ for C_6H_5CN (12, 45, 46), $(2 - 3) \times 10^{-10}$ for C_6H_5CCH (16), and $[(5 - 20) \times 10^{-11}$ for $C_{10}H_7CN$ (6, 12)]. *Third*, the peak fractional abundances of the molecular building blocks and hence precursors of the cyclic compounds, i.e., propargyl (C_3H_3) (47), vinylacetylene (C_4H_4) (10, 48), cyanoacetylene (HCCCN) (49, 50), vinyl cyanide (C_2H_3CN) (48), and cyano substituted propylene isomers (C_3H_5CN) (51), are also included in the model. These results are close to the observed data (*SI Appendix*, Figs. S5 and S6), thus highlighting the performance of our astrochemical model (*SI Appendix*, Table S6). *Finally*, peak abundances of $(1.8 \pm 0.2) \times 10^{-10}$ (3.9×10^5 y) and $(5.4 \pm 0.3) \times 10^{-10}$ (2.5×10^5 y) of ethynylindene (C_9H_7CCH) and ethynylnaphthalene ($C_{10}H_7CCH$) are also projected; these are significantly larger than those of the corresponding cyano-substituted species. These results suggest that ethynylindene (C_9H_7CCH) and ethynylnaphthalene ($C_{10}H_7CCH$) (44) are promising candidates for astronomical detections in TMC-1 via the Yebes 40 m radio telescope (10) and/or the Green Bank Telescope (GBT) (6).

Conclusions

To conclude, our combined experimental, computational, and astrochemical modeling study affords persuasive evidence of the low-temperature formation of cyclopentadiene (C_5H_6) predominantly via the CH—C_4H_6 reaction in TMC-1. The model predicts a peak concentration of C_5H_6 in TMC-1 within 20% of the observed abundances. Both the model predictions and the observations have uncertainties larger than 20%. The CH radical is detected in TMC-1 with high abundances of $(3.0 \pm 1.0) \times 10^8$ (52, 53). The principal source of CH in TMC-1 is likely to be the dissociative recombination of hydrocarbon ions, in particular CH_3^+, e.g.: $CH_3^+ + e^- \rightarrow CH + H_2$ and $CH_3^+ + e^- \rightarrow CH + H + H$. $CH_2 + H \rightarrow CH + H_2$ also represents main production pathways (53). The photolysis of methane could be important in these processes (54, 55). Up to now, it has been revealed that reactions of CH_3 and CH_2 in their doublet and triplet electronic ground states with hydrocarbons are closed in TMC-1 because of the significant entrance barriers (35). Second, the possible C2+C3 pathways to cylcopentadiene including C_2H+C_3H_6, C_2H_2+C_3H_5, C_2H_3+C_3H_4, C_2H_4+C_3H_3, and C_2H_6+C_3H have been investigated experimentally and theoretically, but cyclopentadiene represents the minor product in the reaction of C_2H+C_3H_6 (56), and the rest reactions are revealed to be closed in low-temperature conditions considering the high entrance barrier (35, 57, 58). The key roles of cyclopentadiene in fundamental low-temperature molecular mass growth processes to PAHs along with their precursors in cold molecular clouds such as in TMC-1 are proposed. Through the simultaneous prediction and hence replication of fractional abundances of close to 20 hydrocarbons along with their nitriles, the astrochemical model provides critical constraints on key reaction pathways involving cyclopentadiene (C_5H_6), thus providing a paradigm shift converting acyclic hydrocarbons to hydrocarbon rings in cold molecular clouds (43). The exploration of the CH—C_4H_6 system is also appealing from the viewpoint of physical organic chemistry. The gas-phase pathway to cyclopentadiene (C_5H_6) represents a universal template toward the formation of substituted cyclopentadiene (C_5H_5R) with R being organic groups such as CN and CCH through reactions of CH with substituted 1,3-butadienes (C_4H_5R). Finally, our study also predicts that the hitherto elusive ethynylindene (C_9H_7CCH) and ethynylnaphthalene ($C_{10}H_7CCH$) isomers may be detectable in TMC-1 (44). Future astronomical searches via Yebes 40 m radio telescope (51) and the GBT (6) would be invaluable to derive their fractional abundances and to contrast those with our modeling predictions. Overall, our investigations provide knowledge of the unusual low-temperature hydrocarbon chemistry involving five-membered ring closure and molecular mass growth, which might help close the gap between astronomical observational and laboratory results of the chemistries. As evidenced here, this elementary reaction triggers a complex chain of neutral–neutral reactions synthesizing an inventory of organic rings in TMC-1, thus bringing us closer to an understanding of the carbonaceous Universe we live in.

Materials and Methods

Crossed Molecular Beams. The gas-phase reactions of CH ($X^2\Pi$) and CD ($X^2\Pi$) with C_4H_6 (X^1A_g) were performed in a crossed molecular beam machine (25, 59). The supersonic beams of CH and CD were generated through photodissociation of bromoform ($CHBr_3$; Aldrich; ≥99%) and d1-bromoform ($CDHBr_3$; Aldrich; ≥99%) with a pulsed 248 nm output from a KrF (Nova Gas) excimer laser (COMPex 110; 30 Hz). The precursors are held in a stainless-steel bubbler and purified via multiple freeze-pump-thaw procedures. The bubbler is kept at 283 K and the precursors are seeded in a 3:1 mixture of neon (Ne; 99.999%; Matheson) and helium (He; 99.999%; Airgas) at 2.2 atm. The peak velocities of the derived CH and CD beams are 991 ± 22 m s^{-1} and 986 ± 19 m s^{-1}, respectively (*SI Appendix*, Table S1). To reduce the velocity, the secondary 1,3-budatene is anti-seeded (10%) in krypton (Praxair, 99.999%) and released by a Proch–Trickl pulse valve utilizing a piezoelectric disc translator (Physik Instrumente, P-286.23) with a backing pressure of 550 Torr (445 ± 17 m s^{-1}). After the skimmer and chopper wheel, the selected CH/CD beams crossed the C_4H_6 beam perpendicularly in the interaction region, resulting in a collision energy of around 6 kJ mol^{-1} (6.2 ± 0.3 kJ mol^{-1} for CH—C_4H_6 system and 6.5 ± 0.3 kJ mol^{-1} for CD—C_4H_6 system) and a Θ_{CM} (CM angle) of around 60° (61.5°± 0.6° for CH—C_4H_6 system and 59.7°± 0.5° for CD—C_4H_6 system) (*SI Appendix*, Table S1). To reduce the background signal from the straight-through molecules, the primary and secondary beams pass

through cold shield (10 K) before colliding. The whole detector is rotatable within the plane defined by the primary and secondary sources to collect the TOF spectra at desired angles. After electron-impact ionization (60), the products of the CH/CD—C_4H_6 reaction were monitored using a triply differentially pumped QMS detector (Extrel, QC 150) in TOF mode (61) (recording the flight time of a selected, well-defined m/z from the interaction region to the detector) under ultrahigh-vacuum conditions (7×10^{-12} Torr). The produced ions first cause a cascade of secondary electrons via a high-voltage aluminum-coated target (−22.5 kV). Then the photon pulses are generated via an organic scintillator and collected by a photomultiplier tube (PMT; Burle; 8850). A forward convolution method was employed to fit the data and extract the reaction dynamics information. To derive the P(ET) (product translational energy), the T(Θ) (angular) flux distributions, the experimental data were transformed into the CM frame from the laboratory reference frame. These CM functions are varied iteratively until best fitting of the laboratory data was achieved (22). The contour flux map, $I(u, \theta) \approx P(u) \times T(\theta)$, which contains the scattering information as a function of the CM velocity u and angle θ represents an image of the collision reaction.

RRKM Calculations. RRKM theory (62–64) calculations were conducted to evaluate energy-dependent rate coefficients for all unimolecular reaction steps on the previously reported C_5H_7 potential energy surface (29) after the initial entrance bimolecular reaction steps. The rate coefficients were assessed as functions of the available internal energy of each intermediate or transition state, which was assumed to be equal to a sum of the collision energy and the energy of chemical activation, which in turn equates to a negative of the relative energy of the species with regard to the CH+C_4H_6 reactants. Molecular parameters derived from the electronic structure calculations were used to compute densities and numbers of states required for the RRKM calculations of the rate coefficients. The calculations were carried out employing our in-house code (65) in the limit of zero pressure corresponding to single-collision conditions. Finally, the computed RRKM rate coefficients were utilized to obtain product branching ratios within steady-state approximation (66).

Astrochemical Modeling. Our astrochemical modeling was operated exploiting a revised UMIST Databases, which contains 737 species, 17 elements, and 8,767 individual reactions (neutral–neutral, ion–neutral, cosmic-ray proton, collisional dissociation, etc.) (41, 67). The bimolecular reactions and photodissociation processes identified are incorporated into the revised modeling (*SI Appendix*, Table S5). To explore the effects of neutral–neutral chemistry to the formation of cyclopentadiene (C_5H_6), and the prototype mono- and bicyclic molecules of benzene (C_6H_6), indene (C_9H_8), naphthalene ($C_{10}H_8$), along with their CN and CCH substituted species in cold molecular cloud of TMC-1 from the simplest acyclic precursors, we constructed a chemical network by expanding the UMIST network with rapid and barrierless neutral–neutral reactions (*SI Appendix*, Table S5) (41). The reaction rate coefficients and (preexponential) factors α (s^{-1}) in the table are parameterized according to the usual Arrhenius-type formula for two-body reactions (41). Additional reactions necessary were included to describe the destruction of molecules by photodissociation involving the photons generated via cosmic-ray interactions. Physical parameters are based on refs. 19, 41, and 42: a temperature of 10 K, a standard cosmic ray ionization rate of 1.3×10^{-17} s^{-1}, a number density of molecular hydrogen of 10^4 cm^{-3}, and a visual extinction of 10 Mag. To derive the quantitative results, first, a fiducial time-dependent gas-phase model was run until the system evolves to the steady state (typically at 10^7 y). The derived abundances of the relevant molecules at this stage are utilized as the initial input for the next step. Second, multiple runs of the simulation were conducted involving the ice mantle species injected via reactive desorption into the gas phase until the steady state is ultimately reached (11). The derived results of the relevant species via our gas-grain chemical model were finally benchmarked with the astronomically observed fractional abundances (*SI Appendix*, Table S6).

Data, Materials, and Software Availability. All study data are included in the article and/or *SI Appendix*.

ACKNOWLEDGMENTS. This work was supported by the U.S. Department of Energy, Basic Energy Sciences, by Grant No. DE-FG02-03ER15411 to the University of Hawaii at Manoa. X.L. acknowledges support from the Natural Science Foundation of Xinjiang Uygur Autonomous Region (No. 2024D01E37) and the NSF of China (12473025).

Author affiliations: [a]Department of Chemistry, University of Hawai'i at Manoa, Honolulu, HI 96822; [b]Laboratory of Combustion Physics and Chemistry, Samara National Research University, Samara 443086, Russia; [c]Department of Chemistry and Biochemistry, Florida International University, Miami, FL 33199; [d]Xinjiang Astronomical Observatory, Chinese Academy of Sciences, Urumqi, Xinjiang 830011, People's Republic of China; [e]Key Laboratory of Radio Astronomy, Chinese Academy of Sciences, Urumqi, Xinjiang 830011, People's Republic of China; and [f]Key Laboratory of Radio Astronomy and Technology, Chinese Academy of Sciences, Beijing 100101, People's Republic of China

Author contributions: R.I.K. designed research; Z.Y., I.A.M., S.J.G., A.A.N., A.M.M., and X.L. performed research; Z.Y. analyzed data; and Z.Y. and R.I.K. wrote the paper.

1. A. Leger, J. Puget, Identification of the "unidentified" IR emission features of interstellar dust? *Astron. Astrophys.* **137**, L5–L8 (1984).
2. A. G. G. M. Tielens, Interstellar polycyclic aromatic hydrocarbon molecules. *Annu. Rev. Astron. Astrophys.* **46**, 289–337 (2008).
3. R. I. Kaiser, N. Hansen, An aromatic universe–A physical chemistry perspective. *J. Phys. Chem. A* **125**, 3826–3840 (2021).
4. B. A. McGuire, 2021 census of interstellar, circumstellar, extragalactic, protoplanetary disk, and exoplanetary molecules. *Astrophys. J. Suppl.* **259**, 30 (2022).
5. J. Cernicharo *et al.*, Discovery of benzyne, o-C_6H_4, in TMC-1 with the QUIJOTE line survey. *Astron. Astrophys.* **652**, L9 (2021).
6. B. A. McGuire *et al.*, Detection of two interstellar polycyclic aromatic hydrocarbons via spectral matched filtering. *Science* **371**, 1265–1269 (2021).
7. A. G. G. M. Tielens, The molecular universe. *Rev. Mod. Phys.* **85**, 1021 (2013).
8. P. Thaddeus, J. Vrtilek, C. Gottlieb, Laboratory and astronomical identification of cyclopropenylidene, C_3H_2. *Astrophys. J.* **299**, L63–L66 (1985).
9. J. Cernicharo *et al.*, Pure hydrocarbon cycles in TMC-1: Discovery of ethynyl cyclopropenylidene, cyclopentadiene, and indene. *Astron. Astrophys.* **649**, L15 (2021).
10. J. Cernicharo *et al.*, Discovery of fulvenallene in TMC-1 with the QUIJOTE line survey. *Astron. Astrophys.* **663**, L9 (2022).
11. B. M. Jones *et al.*, Formation of benzene in the interstellar medium. *Proc. Natl. Acad. Sci. U.S.A.* **108**, 452–457 (2011).
12. A. M. Burkhardt *et al.*, Discovery of the pure polycyclic aromatic hydrocarbon indene (c-C_9H_8) with GOTHAM observations of TMC-1. *Astrophys. J. Lett.* **913**, L18 (2021).
13. M. L. Sita *et al.*, Discovery of interstellar 2-cyanoindene (2–C_9H_7CN) in GOTHAM observations of TMC-1. *Astrophys. J. Lett.* **938**, L12 (2022).
14. R. I. Kaiser *et al.*, Gas-phase synthesis of racemic helicenes and their potential role in the enantiomeric enrichment of sugars and amino acids in meteorites. *Phys. Chem. Chem. Phys.* **24**, 25077–25087 (2022).
15. M. C. McCarthy *et al.*, Interstellar detection of the highly polar five-membered ring cyanocyclopentadiene. *Nat. Astron.* **5**, 176–180 (2021).
16. J. Cernicharo *et al.*, Discovery of two isomers of ethynyl cyclopentadiene in TMC-1: Abundances of CCH and CN derivatives of hydrocarbon cycles. *Astron. Astrophys.* **655**, L1 (2021).
17. F. Zhang *et al.*, Formation of the phenyl radical [$C_6H_5(X^2A_1)$] under single collision conditions: A crossed molecular beam and ab initio study. *J. Am. Chem. Soc.* **132**, 2672–2683 (2010).
18. K. L. Caster, T. M. Selby, D. L. Osborn, S. D. Le Picard, F. Goulay, Product detection of the CH ($X^2\Pi$) radical reaction with cyclopentadiene: A novel route to benzene. *J. Phys. Chem. A* **125**, 6927–6939 (2021).
19. Z. Yang *et al.*, Gas-phase formation of the resonantly stabilized 1-indenyl ($C_9H_7^•$) radical in the interstellar medium. *Sci. Adv.* **9**, eadi5060 (2023).
20. C. He *et al.*, Exotic reaction dynamics in the gas-phase preparation of anthracene ($C_{14}H_{10}$) via spiroaromatic radical transients in the indenyl–cyclopentadienyl radical–radical reaction. *J. Am. Chem. Soc.* **145**, 3084–3091 (2023).
21. A. G. G. M. Tielens, L. J. Allamandola, *Cool Interstellar Physics and Chemistry* (Jenny Stanford Publishing, 2011).
22. R. D. Levine, *Molecular Reaction Dynamics* (Cambridge University Press, Cambridge, UK, 2005).
23. M. F. Vernon, "Molecular beam scattering," Ph.D. Thesis, University of California, Berkeley, CA (1983).
24. P. S. Weiss, "Reaction dynamics of electronically excited alkali atoms with simple molecules," Ph.D Thesis, University of California, Berkeley, CA (1986).
25. X. Gu, Y. Guo, F. Zhang, A. M. Mebel, R. I. Kaiser, Reaction dynamics of carbon-bearing radicals in circumstellar envelopes of carbon stars. *Faraday Discuss.* **133**, 245–275 (2006).
26. B. Ruscic *et al.*, Active thermochemical tables: Thermochemistry for the 21st century. *J. Phys. Conf. Ser.* **16**, 561 (2005).
27. S. J. Klippenstein, L. B. Harding, B. Ruscic, Ab initio computations and active thermochemical tables hand in hand: Heats of formation of core combustion species. *J. Phys. Chem. A* **121**, 6580–6602 (2017).
28. W. B. Miller, S. A. Safron, D. R. Herschbach, Exchange reactions of alkali atoms with alkali halides: A collision complex mechanism. *Discuss. Faraday Soc.* **44**, 108–122 (1967).
29. C. He *et al.*, Gas-phase synthesis of 3-vinylcyclopropene via the crossed beam reaction of the methylidyne radical (CH; $X^2\Pi$) with 1, 3-butadiene ($CH_2CHCHCH_2$; X^1A_g). *ChemPhysChem* **21**, 1295–1309 (2020).
30. R. I. Kaiser, H. Y. Lee, A. M. Mebel, Y. T. Lee, The formation of isomers as potential key intermediates C_5H_5 to polycyclic aromatic hydrocarbon like molecules. *Astrophys. J.* **548**, 852–860 (2001).
31. J. Saltiel, D. F. Sears, A. M. Turek, UV spectrum of the high energy conformer of 1, 3-butadiene in the gas phase. *J. Phys. Chem. A* **105**, 7569–7578 (2001).
32. J. H. Baraban *et al.*, The Molecular structure of gauche-1, 3-butadiene: Experimental establishment of non-planarity. *Angew. Chem. Int. Ed. Engl.* **57**, 1821–1825 (2018).
33. J. Zhang, E. F. Valeev, Prediction of reaction barriers and thermochemical properties with explicitly correlated coupled-cluster methods: A basis set assessment. *J. Chem. Theory Comput.* **8**, 3175–3186 (2012).

34. A. Canosa, I. R. Sims, D. Travers, I. W. M. Smith, B. R. Rowe, Reactions of the methylidine radical with CH_4, C_2H_2, C_2H_4, C_2H_6, and but-1-ene studied between 23 and 295 K with a CRESU apparatus. *Astron. Astrophys.* **323**, 644–651 (1997).
35. R. I. Kaiser, Experimental investigation on the formation of carbon-bearing molecules in the interstellar medium via neutral— neutral reactions. *Chem. Rev.* **102**, 1309–1358 (2002).
36. N. Daugey *et al.*, Kinetic measurements on methylidyne radical reactions with several hydrocarbons at low temperatures. *Phys. Chem. Chem. Phys.* **7**, 2921–2927 (2005).
37. H. Thiesemann, E. P. Clifford, C. A. Taatjes, S. J. Klippenstein, Temperature dependence and deuterium kinetic isotope effects in the CH (CD)+ C_2H_4 (C_2D_4) reaction between 295 and 726 K. *J. Phys. Chem. A* **105**, 5393–5401 (2001).
38. S. Doddipatla *et al.*, Low-temperature gas-phase formation of indene in the interstellar medium. *Sci. Adv.* **7**, eabd4044 (2021).
39. D. Damiani, L. Ferretti, E. Gallinella, Structure of cyclopentadiene from microwave spectra of several deuterated species. *Chem. Phys. Lett.* **37**, 265–269 (1976).
40. W. Caminati, Low-energy vibrations of indene. *J. Chem. Soc. Faraday Trans.* **89**, 4153–4155 (1993).
41. D. McElroy *et al.*, The UMIST database for astrochemistry 2012. *Astron. Astrophys.* **550**, A36 (2013).
42. A. J. Markwick, T. J. Millar, S. B. Charnley, On the abundance gradients of organic molecules along the TMC-1 ridge. *Astrophys. J.* **535**, 256 (2000).
43. M. Agúndez, N. Marcelino, B. Tercero, J. Cernicharo, Aromatic cycles are widespread in cold clouds. *Astron. Astrophys.* **677**, L13 (2023).
44. C. Cabezas, I. Peña, J. Cernicharo, Laboratory rotational spectroscopy and astronomical search of ethynyl substituted naphthalene. *Mon. Not. R. Astron. Soc.* **519**, 2590–2597 (2023).
45. B. A. McGuire *et al.*, Detection of the aromatic molecule benzonitrile (c-C_6H_5CN) in the interstellar medium. *Science* **359**, 202–205 (2018).
46. A. M. Burkhardt *et al.*, Ubiquitous aromatic carbon chemistry at the earliest stages of star formation. *Nat. Astron.* **5**, 181–187 (2021).
47. M. Agúndez *et al.*, Detection of the propargyl radical at λ 3 mm. *Astron. Astrophys.* **657**, A96 (2022).
48. J. Cernicharo *et al.*, Discovery of CH2CHCCH and detection of HCCN, HC4N, CH3CH2CN, and tentatively, CH3CH2CCH in TMC-1. *Astron. Astrophys.* **647**, L2 (2021).
49. W. D. Langer, F. P. Schloerb, R. L. Snell, J. S. Young, Detection of deuterated cyanoacetylene in the interstellar cloud TMC 1. *Astrophys. J.* **239**, L125–L128 (1980).
50. J. Cernicharo *et al.*, Discovery of HC_4NC in TMC-1: A study of the isomers of HC_3N, HC_5N, and HC_7N. *Astron. Astrophys.* **642**, L8 (2020).
51. J. Cernicharo *et al.*, Discovery of five cyano derivatives of propene with the QUIJOTE line survey. *Astron. Astrophys.* **663**, L5 (2022).
52. Y. Sheffer *et al.*, Ultraviolet survey of CO and H_2 in diffuse molecular clouds: The reflection of two photochemistry regimes in abundance relationships. *Astrophys. J.* **687**, 1075 (2008).
53. A. Suutarinen *et al.*, CH abundance gradient in TMC-1. *Astron. Astrophys.* **531**, A121 (2011).
54. R. E. Rebbert, P. Ausloos, Photolysis of methane: Quantum yield of $C(^1D)$ and CH. *J. Photochem.* **1**, 171–176 (1972).
55. B. Gans *et al.*, Photolysis of methane revisited at 121.6 nm and at 118.2 nm: Quantum yields of the primary products, measured by mass spectrometry. *Phys. Chem. Chem. Phys.* **13**, 8140–8152 (2011).
56. S. J. Goettl *et al.*, Gas-phase study of the elementary reaction of the D1-ethynyl radical (C_2D; $X^2\Sigma^+$) with propylene (C_3H_6; X^1A') under single-collision conditions. *J. Phys. Chem. A* **126**, 1889–1898 (2022).
57. J. Bouwman, A. Bodi, J. Oomens, P. Hemberger, On the formation of cyclopentadiene in the $C_3H_5^+ + C_2H_2$ reaction. *Phys. Chem. Chem. Phys.* **17**, 20508–20514 (2015).
58. M. Saeys, M.-F. Reyniers, G. B. Marin, V. Van Speybroeck, M. Waroquier, Ab initio calculations for hydrocarbons: Enthalpy of formation, transition state geometry, and activation energy for radical reactions. *J. Phys. Chem. A* **107**, 9147–9159 (2003).
59. Z. Yang *et al.*, Gas-Phase Formation of 1, 3, 5, 7-cyclooctatetraene (C_8H_8) through ring expansion via the aromatic 1, 3, 5-cyclooctatrien-7-yl radical ($C_8H_9^•$) transient. *J. Am. Chem. Soc.* **144**, 22470–22478 (2022).
60. G. O. Brink, Electron bombardment molecular beam detector. *Rev. Sci. Instrum.* **37**, 857–860 (1966).
61. N. R. Daly, Scintillation type mass spectrometer ion detector. *Rev. Sci. Instrum.* **31**, 264–267 (1960).
62. P. J. Robinson, K. A. Holbrook, *Unimolecular Reactions* (Wiley-Interscience, London and New York, 1972).
63. H. Eyring, S. H. Lin, S. M. Lin, *Basic Chemical Kinetics* (John Wiley & Sons, New York, Chichester, Brisbane, Toronto, 1980).
64. J. I. Steinfeld, J. S. Francisco, W. L. Hase, *Chemical Kinetics and Dynamics* (Prentice Hall, Upper Saddle River, NJ, 1999).
65. C. He *et al.*, Elucidating the chemical dynamics of the elementary reactions of the 1-propynyl radical (CH_3CC; X^2A_1) with methylacetylene (H_3CCCH; X^1A_1) and allene (H_2CCCH_2; X^1A_1). *J. Phys. Chem. A* **123**, 5446–5462 (2019).
66. V. V. Kislov, T. L. Nguyen, A. M. Mebel, S. H. Lin, S. C. Smith, Photodissociation of benzene under collision-free conditions: An ab initio/Rice–Ramsperger–Kassel–Marcus study. *J. Chem. Phys.* **120**, 7008–7017 (2004).
67. T. J. Millar, C. Walsh, M. Van de Sande, A. J. Markwick, The UMIST database for astrochemistry 2022. *Astron. Astrophys.* **682**, A109 (2024).